2593. Rubbing dynamics behavior of a flywheel shafting with a single point flexible support

Changliang Tang[1], Dongjiang Han[2], Jinfu Yang[3]
Institute of Engineering Thermophysics, Chinese Academy of Sciences, Beijing, 100190, China
[1]Corresponding author
E-mail: [1]*tangcl08@mails.tsinghua.edu.cn*, [2]*handongjiang@iet.cn*, [3]*yangjinfu@iet.cn*

Received 13 April 2017; received in revised form 13 August 2017; accepted 28 August 2017
DOI https://doi.org/10.21595/jve.2017.18480

Abstract. The flywheel energy storage system is a new kind conversion device which realizes electric energy and kinetic energy transform into each other. The dynamic characteristics of flywheel energy storage system have been studied extensively in recent years. A single point flexible support is suitable for the small flywheel system, because the friction loss is very low. The flywheel spin test system with a single point flexible support was built. The dynamic model of the flywheel shafting was established to calculate the critical speeds, modal shape and modal damping ratio at different speeds. The results show that the dynamic characteristics of the flywheel shaft are stable, and its structure is simple and efficient. The comparison between the calculated unbalance response and the experimental response indicates that the dynamic model is appropriate. When the flywheel started up and rotated at different speeds, the rubbing dynamics behavior was obtained by the experiment. Full rubbing occurred at high speed would damage the flywheel and stop, which should be tried to avoid.

Keywords: spin test, stop, rubbing to start up, excitation frequency, stability.

Nomenclature

r_1	Vibration displacement of the oil damper
r_2	Vibration displacement of the flywheel bottom
r_3	Vibration displacement of the flywheel top
x_c, y_c	Coordinates of mass centric
x_1, y_1	Vibration displacement of the oil damper
x_2, y_2	Vibration displacement of the flywheel bottom
x_3, y_3	Vibration displacement of the flywheel top
c_1	Damping coefficient of the oil damper
c_3	Damping coefficient of the stop
k_1	Stiffness of the oil damper
k_2	Stiffness of the pivot
k_3	Stiffness of the stop
l	Length of the flywheel
l_1	Length between mass center and its upper end
l_2	Length between mass center and its lower end
l_s	Length of the pivot
J_p	Polar moment inertia of the flywheel
J_d	Diameter moment inertia of the flywheel
m_1	Mass of the oil damper
M	Mass of the flywheel

1. Introduction

The flywheel energy storage system is a new kind conversion device which realizes electric energy and kinetic energy transform into each other [1]. The flywheel rotor is driven to high speed by motor when electric energy is surplus. The rotating kinetic energy will be converted into electric energy by the flywheel deceleration when needed. The flywheel energy storage is a purely physical energy storage, which has great advantages of high efficiency, high instantaneous power,

fast depth charge and discharge, long service life, little pollution. It is the most promising one of the energy storage technology. at present, the flywheel energy storage technology has been applied to the power grid frequency modulation, peak load shifting, rail braking kinetic energy regeneration, uninterruptible power supply (UPS), high power pulse power, satellite energy storage / attitude control and many other areas [2-4]. The flywheel energy storage technology may be used in energy management of network base station in the future [5-9].

Many scholars have done a lot of work on the strength theory and design of the composite flywheel [10-13]. However, their investigations are limited to theoretical analyses and calculations, and shorted of spin tests, which is mainly because of great difficulty in motor technology and bearing technology. to carry out the flywheel spin test efficiently, it is necessary to establish a spin test system which is stable, simple, and easy to regulate speed and suitable for longtime operation. The flywheel shafting system generally uses the super-critical rotor dynamic design. However, the flywheel rotor keeps its rigid state in sub-critical.

Based on the dynamics theory of super-critical operation above, it could be seen from Fig. 1 that we designed and established a flywheel shafting for spin test, whose lower support was composed of a very flexible pivot-jewel bearing [14-16] and an oil damper. Obviously, the flywheel shafting was unstable when it started up. a stop was designed and installed inside the flywheel hollow top. There was a suitable gap between the stop and flywheel rotor. The gap was very small, and the order of magnitude was about several hundred microns. The stop was used to suppress the vibration amplitude when it exceeded the gap. When the flywheel started up, the stop would act. Rubbing and friction would happen inside the gap. With the increase of rotating speed, gyroscopic effect of flywheel was becoming larger and larger, and rubbing and friction inside the gap could absorb a large amount of vibration energy from the flywheel vibration. Then flywheel was rotating stably. After the flywheel started up, the stop did not act due to the gap was much larger than vibration amplitude by residual unbalance. The stiffness of the stop is usually much higher than that of the flexible pivot-jewel bearing. The system has simple structure and very low cost, which is very suitable for the flywheel spin test.

The idea of using a stop to limit the vibration of the mechanical system has been around for a long time. the stop is used to absorb vibration and limit movement. There are many studies in this area in the last several decades [17-20]. However, using stops to limit and absorb vibration energy of flywheel when it starts up is a new idea. the stop is used to provide support by rubbing for the flywheel when it starts up. The rubbing inside the gaps would cause the rotating shafting to have strong non-linear characteristics. Most studies have shown that rubbing is a detrimental dynamic phenomenon that caused the rotating shafting to be in an unstable and easily damaged state [21-25]. There is little research on how to use rubbing effectively to realize the stability of the rotor bearing system, especially for a flywheel rotor with large gyroscope effect.

This paper is written to investigate the rubbing mechanism of enhancing the stability of rotor. Compared with theoretical analysis, the experimental results of the dynamic characteristics of rotor bearing systems with rubbing are fewer. The rubbing experiments are difficult to carry out as well as dangerous. The rubbing dynamics of the rotor system, especially the relationship between full rubbing and stability is still unclear, and the results of experiments on full rubbing are absent in publications. The dynamic model of the flywheel-bearing-damper system was built by means of the Lagrangian equation. The Campbell diagram, critical speeds, mode shapes, and modal damping ratios were calculated at different speeds. When the flywheel started up and rotated at different speeds, the rubbing dynamics behavior was obtained by the experiment. The results of this research are valuable for studying the mechanism of rubbing and stability, although these studies are relatively preliminary.

2. Dynamic model of the flywheel bearing system

2.1. Spin test system diagram and its dynamic model

Fig. 1 shows a diagram of the flywheel spin test system, which is composed of the flywheel rotor, stop, disk type motor, pivot-jewel bearing, oil damper and some vibration sensors. The whole spin test system is installed in a vacuum container. a stop is designed and installed inside the flywheel hollow top. There is a suitable gap between the stop and flywheel rotor. The gap is very small, and the order of magnitude is about several hundred microns. The stop is used to suppress the vibration amplitude when it exceeds the gap. When the flywheel starts up, the stop will act, especially when the flywheel is beginning to accelerate.

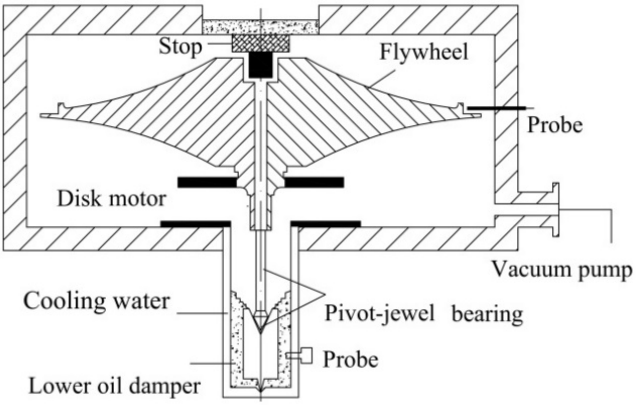

Fig. 1. The flywheel shafting system

The designed stop controls vibrations inside the gap. The vibration energy will be absorbed and dissipated by collision and friction when the flywheel starts up. Because the stiffness of pivot is very small, the stiffness of the stop is designed much higher.

The disk type motor is composed of disk type rotor and disk type stator. The disk type rotor is integrated with the flywheel rotor, and the structure is very compact. The heat produced by disk stator is transferred by a cooling system which is also used by the lower oil damper.

The pivot jewel bearing is lubricated with oil baths. The pivot top is directly inside the lubricating oil. The diameter of the circular arc at the top of the pivot is only 2 mm, and contact area between pivot top and jewel bearing is less than 1.5 mm^2. The friction loss is very small. The pivot is made of high temperature carbon steel, and the jewel material is corundum, so the service life of pivot jewel bearing is very long, which is about tens of thousands of hours. The pivot jewel bearing can be used in the super high vacuum environments. the jewel bearing is set on the top of damping body which connects the mechanical housing with three flexible springs. The springs provide radial stiffness for the low support of the flywheel. the viscosity of the oil in the damper is relatively large, which provides viscous damping effect for the lower support of the flywheel. Obviously, viscous damping can suppress flywheel vibration, and can also lubricate bearings and dissipate friction heat.

The flywheel shafting has no upper support, so the lower damper is very important for dynamic characteristics. Based on its working principle, the damper is simplified to spring-oscillator model with a single degree of freedom. the eddy current sensor installed inside the shell of damper is used to measure the vibration response of damping body by excitation. The equivalent mass, stiffness and damping coefficient of the lower damper can be derived according to vibration theory of the single degree of freedom.

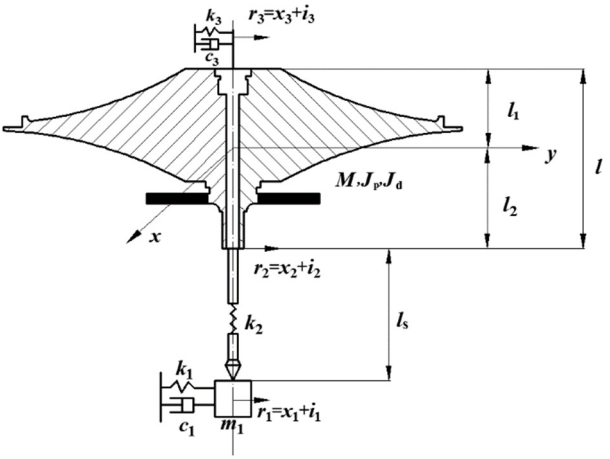

Fig. 2. The dynamic model

The dynamic model is as shown in Fig. 2. in order to simulate conveniently, the complex vibration displacement $r(r = x + iy)$ is used to represent the vibration displacements in the x and y directions. the symbols in Fig. 2 are listed in the Nomenclature.

2.2. The dynamics modeling of the flywheel shafting system

The dynamic model of flywheel shafting system is as shown in Fig. 2. The rotating kinetic function T_i, the potential energy function U_i, and the consumed energy function Z_i are obtained by Lagrangian equation.

1) The spring squeeze film damper:

$$\begin{aligned} T_1 &= \frac{1}{2}m_1\left(\dot{x}_1{}^2 + \dot{y}_1{}^2\right), \\ U_1 &= \frac{1}{2}k_1\left(x_1{}^2 + y_1{}^2\right), \\ Z_1 &= \frac{1}{2}c_1\left(\dot{x}_1{}^2 + \dot{y}_1{}^2\right). \end{aligned} \tag{1}$$

2) The pivot has stiffness and no mass:

$$U_{12} = \frac{1}{2}k_2\left\{\left[(x_2 - x_1) - \frac{l_s}{l}(x_3 - x_2)\right]^2 + \left[(y_2 - y_1) - \frac{l_s}{l}(y_3 - y_2)\right]^2\right\}. \tag{2}$$

3) The flywheel:

$$\begin{aligned} T_2 &= \frac{1}{2}M\left(\dot{x}_c{}^2 + \dot{y}_c{}^2\right) + \frac{1}{2}J_p\omega(\omega + 2\dot{\alpha}\beta) + \frac{1}{2}J\left(\dot{\alpha}^2 + \dot{\beta}^2\right), \\ x_c &= \frac{l_2x_3 + l_1x_2}{l},\ \ y_c = \frac{l_2y_3 + l_1y_2}{l},\ \ \alpha = \frac{x_3 - x_2}{l},\ \ \beta = \frac{y_3 - y_2}{l}. \end{aligned} \tag{3}$$

4) The dynamic model when stop acts:

$$\begin{aligned} U_3 &= \frac{1}{2}k_3\left(x_3{}^2 + y_3{}^2\right), \\ Z_3 &= \frac{1}{2}c_3\left(\dot{x}_3{}^2 + \dot{y}_3{}^2\right). \end{aligned} \tag{4}$$

The free vibration equation of the flywheel shafting system is obtained in the matrix form by Lagrange method:

$$[M]\{\ddot{r}\} + ([C] - i\omega[H])\{\dot{r}\} + [K]\{r\} = \{0\}, \tag{5}$$

$$[M] = \begin{bmatrix} m_1 & 0 & 0 \\ 0 & m_2 & m_0 \\ 0 & m_0 & m_3 \end{bmatrix}, \quad [C] = \begin{bmatrix} c_1 & 0 & 0 \\ 0 & 0 & 0 \\ 0 & 0 & c_3 \end{bmatrix}, \quad [H] = \begin{bmatrix} 0 & 0 & 0 \\ 0 & \frac{J_p}{l^2} & -\frac{J_p}{l^2} \\ 0 & -\frac{J_p}{l^2} & \frac{J_p}{l^2} \end{bmatrix},$$

$$[K] = \begin{bmatrix} k_1 + k_2 & -\left(k_2 + \frac{k_2 l_s}{l}\right) & \frac{k_2 l_s}{l} \\ -\left(k_2 + \frac{k_2 l_s}{l}\right) & k_2 + \frac{k_2 {l_s}^2}{l^2} + \frac{2k_2 l_s}{l} & -\left(\frac{k_2 {l_s}^2}{l^2} + \frac{k_2 l_s}{l}\right) \\ \frac{k_2 l_s}{l} & -\left(\frac{k_2 {l_s}^2}{l^2} + \frac{k_2 l_s}{l}\right) & \frac{k_2 {l_s}^2}{l^2} + k_3 \end{bmatrix},$$

$$m_2 = \frac{M{l_1}^2 + J_d}{l^2}, \quad m_3 = \frac{M{l_2}^2 + J_d}{l^2}, \quad m_0 = \frac{Ml_1 l_2 - J_d}{l^2}.$$

The first and second order differential of vibration displacement column vector are represented $\{\dot{r}\}$ and $\{\ddot{r}\}$. $\{r\} = [r_1 \quad r_2 \quad r_3]$, and $r_j = x_j + iy_j$, $(j = 1, 2, 3)$. State vector method can be used to solve Eq. (5), whose solution form is:

$$r_j = R_j e^{st}, \quad (j = 1, 2, 3). \tag{6}$$

The complex vibration amplitudes and complex frequencies are:

$$\begin{aligned} &R_j = X_j + iY_j, \quad (j = 1, 2, 3), \\ &s = \lambda + i\omega. \end{aligned} \tag{7}$$

In which, λ is the mode decaying exponent, $\omega = 2\pi f$ is the mode angular frequency and f is the modal frequency. The modal damping ratio $\zeta = -\lambda/\omega$, and if $\lambda > 0$, the dynamic system is stable. the larger $|\zeta|$ is, the better stability the system has. So, the modal frequencies, mode shapes and modal damping ratios of the flywheel system were obtained by solving Eq. (5). in engineering practice, the flywheel rotor inevitably exists unbalance, if the residual unbalance is $\{f\} = \{u\}\omega^2 e^{i\omega t}$ at the flywheel rotor top, the forced vibration equation of the flywheel dynamic system is got by means of the Lagrangian equation. The steady state unbalance response was calculated from Eq. (8):

$$[M]\{\ddot{r}\} + ([C] - i\omega[H])\{\dot{r}\} + [K]\{r\} = \{u\}\omega^2 e^{i\omega t}. \tag{8}$$

3. The dynamic simulation of the flywheel shafting

The dynamic parameters of the designed flywheel spin test shafting are as follows: $m_1 = 0.02$ kg, $M = 0.6$ kg, $J_p = 5.8\text{e}^{-4}$ kg·m^2, $J_d = 4.1\text{e}^{-4}$ kg·m^2, $l = 66.1$ mm, $l_1 = 25$ mm, $l_2 = 41$ mm, $l_s = 26$ mm, $k_1 = 586$ N/m, $c_1 = 0.29$ N·s/m, $k_2 = 5030$ N/m, $k_3 = 1\text{e}^4$ N/m, $c_3 = 0$ N·s/m.

3.1. Critical speeds

Fig. 3 shows the Campbell diagram. in Fig. 3, '1F' and '1B' indicate the first-order forward and backward whirl of the flywheel respectively. 'LDF' and 'LDB' indicate the forward and backward whirl of the lower damper respectively. '2F' and '2B' indicate the second-order forward

and backward whirl of the flywheel respectively.

From the Fig. 3, the mode frequencies at different speeds are presented. The flywheel rotor is generally flat rotor, which has strong gyroscopic effect due to angular component. The modal frequency varies with the rotating speed. The first-order mode of the flywheel shafting divides into forward and backward modes, as well as the second-order mode. The forward frequency is increased as the speed increases, while the backward frequency is decreased as the speed increases. the shape of the flywheel rotor, the mass and the inertia moment distribution are the main sources of modal frequency variation.

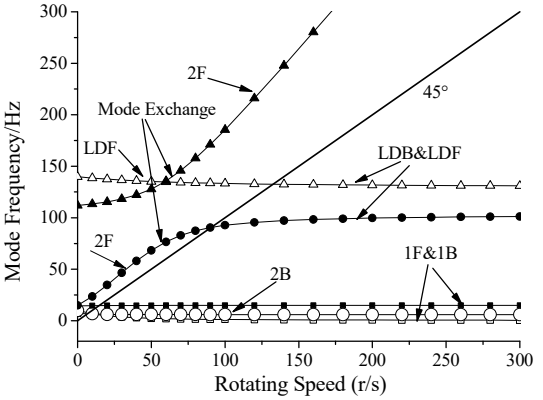

Fig. 3. The Campbell diagram

In this case, the gyroscopic effect mainly affects the second-order modes of the flywheel. The gyroscopic effect essentially enhances the stiffness of the flywheel shafting with the increasing rotating speed for the second-order forward whirl. This effect is just the opposite for the second-order backward whirl. For the first-order modes, the effect is small. The conical mode of the flywheel rotor exchanges with the lower damper mode when it rotates at 4200 rpm-5400 rpm. The exchange of modes completes when the rotating speed exceeds 6000 rpm. When the forward whirl frequency and speed frequency are the same, the corresponding speed is the critical speed, and generally corresponds to the amplitude peak. for the dynamic system as shown in Fig. 2, the critical speeds are 900 rpm (1st mode) and 7800 rpm (Lower damper mode). It is found that the flexible pivot greatly decreases the critical speeds.

3.2. Mode shapes

The mode shapes at the critical speeds are as shown in Fig. 4(a) and Fig. 4(b) respectively: the flywheel top, the flywheel bottom and the lower damper are displayed as three hollow dots from top to bottom in the two figures respectively.

Fig. 3 and Fig. 4 show that the conical mode of the flywheel exchanges with the lower damper mode when modal frequencies are close to each other. The vibration amplitude of the flywheel decreases in the lower damper mode, and it increases in the conical mode. the amplitude of the lower damper gradually decreases in the conical mode. It is the zone of dual mode shapes when in the speed range 900 rpm-7800 rpm. The exchange of modes completes basically when the rotating speed exceeds 6000 rpm.

When the rotating speed is 6000 rpm, the mode shapes of the flywheel shafting are shown in Fig. 5. The flywheel passes through the zones of cylindrical mode and dual modes in the spin test. Compared with conventional bearings, the stiffness of both elastic pivot and lower damper is very small, which makes their mode frequencies so close. The exchange of mode shapes occurs in a narrow frequency range is a new kind of dynamic characteristics produced by flexible damping support.

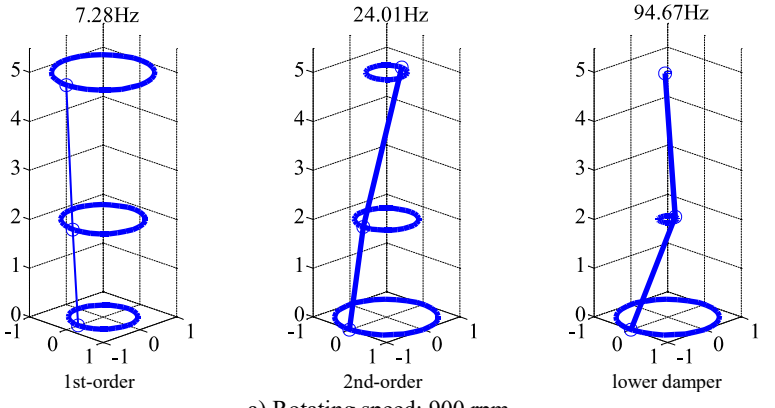

a) Rotating speed: 900 rpm

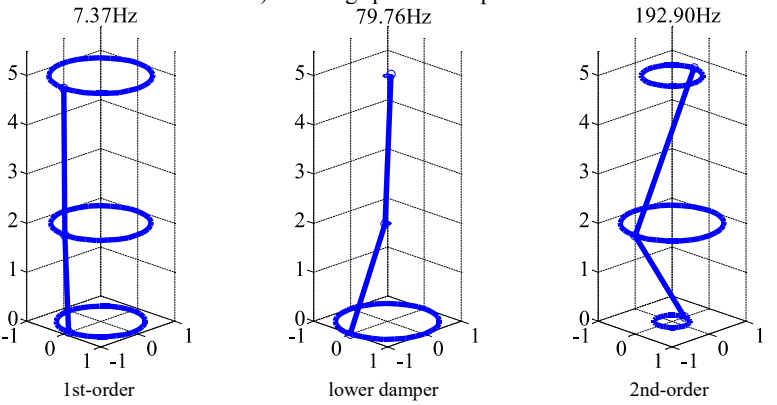

b) Rotating speed: 7800 rpm

Fig. 4. Mode shapes of the flywheel shafting

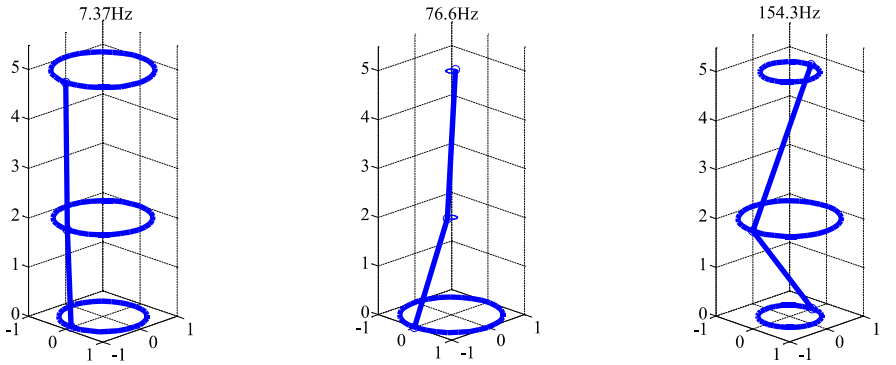

a) b) c)

Fig. 5. Mode shapes (rotating speed: 6000 rpm)

In order to test the flywheel structure strength, rotating speed is generally over 48000 rpm. Fig. 6 shows the mode shapes of the flywheel shafting. The modal frequency of the second-order mode is 1132.9 Hz, which is larger than 800 Hz, so it will not be shown in the test. The lower damper mode shape is displayed as circular motion of damping body, while flywheel is fixed. The first-order mode shape of the flywheel is still cylindrical mode.

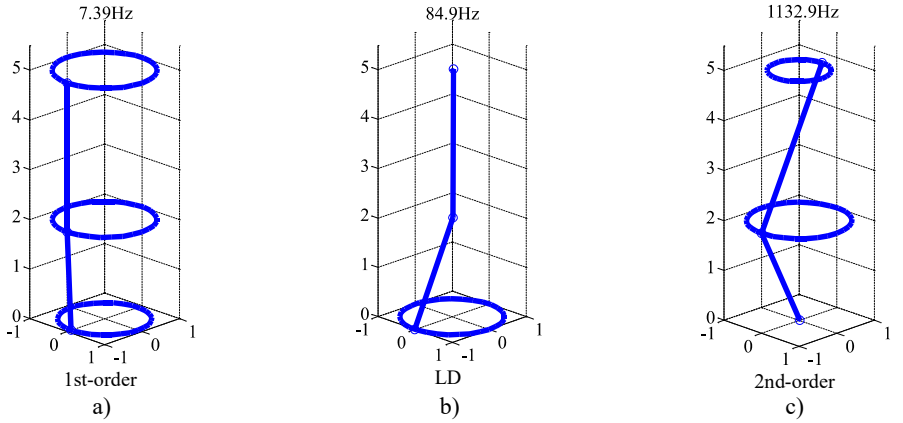

Fig. 6. Mode shapes (rotating speed: 48000 rpm)

3.3. Modal damping ratios

The modal damping is obtained by solving Eq. (5) to assess the stability of the flywheel shafting. The modal damping ratio varies with the rotating speed, which is shown in Fig. 7. Due to no bearing at the flywheel top, the flywheel is leaning against the inside of the flywheel top when the rotating speed is zero. Obviously, the flywheel shafting is unstable when it starts up. with the increase of rotating speed, gyroscopic effect of flywheel is becoming larger and larger, and vibration energy of the flywheel is dissipated quickly through collision and friction inside the gap between the flywheel and stop, then flywheel is rotating stably. k_3 is 10^4 N/m when the stop acts, and k_3 is 0 N/m when flywheel is rotating stably. The modal damping ratios of each mode are obtained when the stop acts or not.

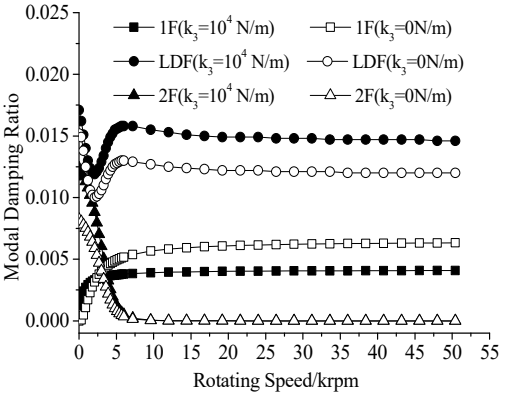

Fig. 7. The modal damping ratios

The dynamics of the flywheel shafting is stable when its modal damping ratios are positive for forward whirl modes. The larger the modal damping ratio is, the faster the complex vibration displacement r attenuates. The system has better dynamic stability. So, the modal damping ratios have an obvious impact on the performance.

Fig. 7 indicates the modal ratio of the first-order mode is becoming larger with the rotating speed is increasing, which is more than 0.005. The modal ratio of the second-order mode is becoming smaller with the rotating speed is dropping. However, it is still positive. Due to the second-order modal frequency is always much higher than its rotating speed, it will not appear in the spin test. The ratio of the lower damper mode is becoming larger with the rotating speed is increasing, and slowing shrieking to 0.012. The stop mainly affects the first-order mode and the

lower damper mode, and plays only a small part on the second-order mode. The flywheel shafting has good stability whether the stop works or not.

4. Experimental verification of dynamic simulation

The experimental set-up was mainly composed of the following three parts: the flywheel shafting system, the test instruments, the data collector and analyzer.

The flywheel shafting system is described in detail in Section 2.1. The test instruments are composed of eddy current displacement sensors and photoelectric speed sensors. The data collector and analyzer are composed of NI DAQ and computer. The functions of test measurement system are vibration measuring, monitoring, data acquisition, and offline analysis. The sensitivity of eddy current displacement sensors is 20 mv/μm, and gap-voltage is –10-10 V, probe diameter is 5 mm, and supply voltage is ±15 V. The channel number of NI DAQ is 16, A/D accuracy is 12 bit, and maximum sampling frequency is 100 kHz. The vibration amplitude is measured by eddy current displacement sensors, and the time domain signal are converted to frequency domain signals through SFFT algorithm.

Two probes are located at the flywheel top to measure the vibration displacement of x and y directions respectively. Two probes are installed in the lower damper to collect the vibration displacement of damping body in x and y directions respectively.

The photoelectric sensor obtains the rotating speed of the rotor. The test data are observed by the computer, analyzed by the NI DAQ. the test flywheel is the origin of the above theoretical model.

4.1. Critical speeds

For theoretical calculation, when the forward whirl frequency and speed frequency are the same, the corresponding speed is the critical speed, and generally corresponds to the amplitude peak. for the dynamic system as shown in Fig. 2 of section 3.1, the critical speeds are 900 rpm (1st mode) and 7800 rpm (Lower damper mode).

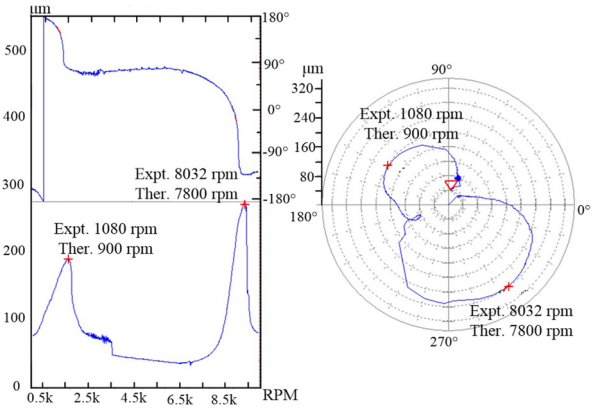

Fig. 8. Critical speeds of the flywheel shafting (lower damper)

For the experiments, the eddy current sensors also installed in the lower damper can measure the forced vibration responses of the damping body. The sensors were installed at central section of the lower damper. the electrical signal by the preamplifier was input to the oscilloscope. The amplitude-frequency curve of the damping body in the lower damper can be obtained by FFT analysis.

Fig. 8 showed the amplitude-frequency response, its Bode map and Nyquist map. The critical speeds would be obtained from Fig. 8. The flywheel ran up to 10000 rpm steadily. The flywheel

shafting system had two critical speeds. The first critical speed was 1080 rpm, whose theoretical result was 900 rpm. The relative error was 16.7 %. the phase angle changed from 180° to 90°. The amplitude at the first critical speed was about 140 μm. The second critical speed was 8032 rpm, whose theoretical result was 7800 rpm. the relative error was just 2.9 %. The phase angle changed from 90° to 135°. The amplitude at the second critical speed was about 256 μm. It was found that the numerical results were close to the measured data, which indicated that the dynamic model well described the dynamic behavior. When the flywheel passed the two critical speeds, the vibration amplitude shrank rapidly with the increase of the speed, which was the self-centering effect of the rotating flywheel.

4.2. The forced vibration response

The residual unbalance of the flywheel rotor was 0.1 g·cm∠37° by dynamic balance test, the steady state unbalance responses could be calculated by Eq. (8). The vibrations of the flywheel shafting were measured at the different damping and stiffness in the experiment, which verified the correctness of the dynamics modeling and simulation.

For the flywheel shafting shown in Fig. 1 and Fig. 2, the stiffness and damping of the lower damper were easier to adjust. the equivalent mass of the damper was determined by the mass of the damping body. The equivalent damping coefficient was determined by the viscosity of the damping medium. The equivalent stiffness was determined by the three small stiffness springs.

Based on its working principle, the damper was simplified to spring-oscillator model with a single degree of freedom. The eddy current sensor installed inside the shell of damper was used to measure the vibration response of damping body by excitation. The equivalent mass, stiffness and damping coefficient of the lower damper could be derived according to vibration theory of the single degree of freedom.

The vacuum oil Mobil 1 and Mobil 68 were used to revise the damping coefficient c_1. The springs with different thickness were chosen to change the stiffness k_1. Four different stiffness and damping coefficients were used to carry out the spin test. the k_1 was 586 N/m or 2546 N/m respectively, and c_1 was 0.7 N·s/m or 1.7 N·s/m. The other dynamic parameters were consistent with ones in section 3.

The eddy current sensors installed in the lower damper can measure the forced vibration responses of the damping body. When c_1 was 0.7 N·s/m or 1.7 N·s/m, and k_1 was 586 N/m, the effect of damping on amplitude – frequency response was shown in Fig. 9.

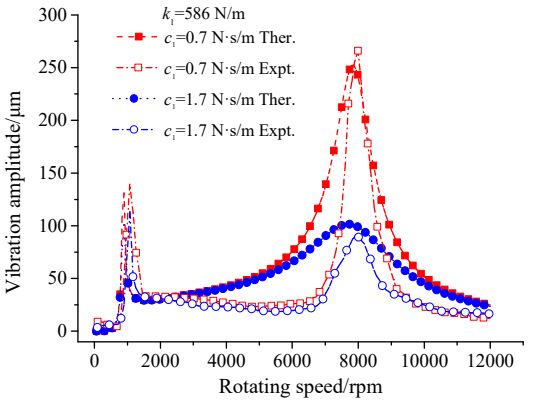

Fig. 9. The effect of damping on amplitude – frequency response

When c_1 was 0.7 N·s/m, the first critical speed measured was 1080 rpm, the theoretical result was 900 rpm, the second critical speed measured was 8032 rpm, the theoretical result was 7800 rpm. When c_1 was 1.7 N·s/m, the critical speeds were almost no change, which showed the

damping coefficient had little effect on the critical speeds of the shafting.

However, increasing damping coefficient could significantly suppress the amplitude of the vibration when the flywheel passed the two critical speeds. Fig. 9 showed the theoretical calculations of the amplitude were in good agreement with values measured in the experiment, especially when speed was near the critical speeds. The experimental values were slightly smaller than the calculated values in the zone away from the critical speeds.

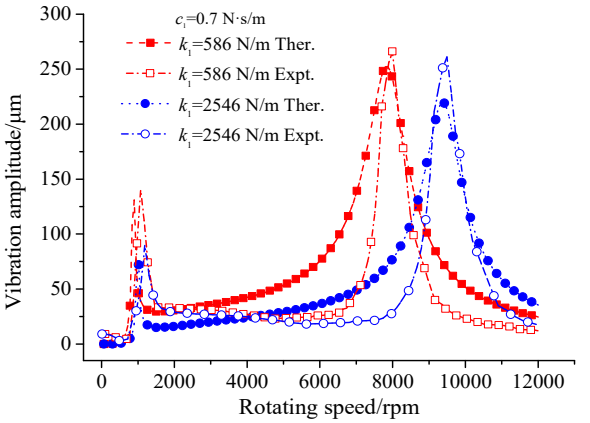

Fig. 10. The effect of stiffness on amplitude – frequency response

Fig. 10 showed the effect of stiffness on amplitude – frequency response. The larger stiffness increased the critical speeds greatly, which made difficulty to pass the critical speeds. The first critical speed increased from 1080 rpm to 1200 rpm, and the second critical speed increased from 8032 rpm to 9652 rpm. The larger stiffness had little effect on the vibration amplitude when passed the second critical speed. However, the larger stiffness could reduce the amplitude when passed the first critical speed, which from 135 μm to 75 μm.

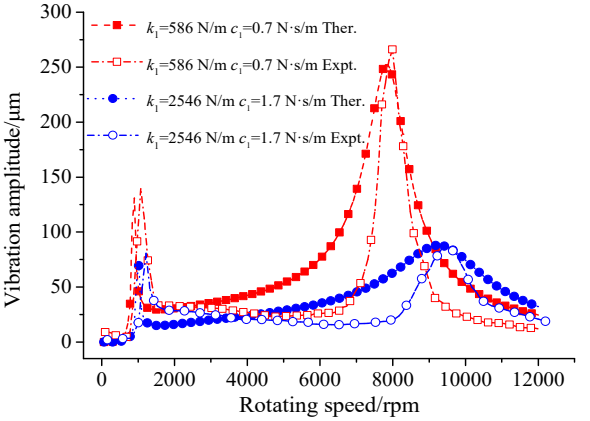

Fig. 11. The combination of stiffness and damping

Through the above discussion, the larger damping mainly suppressed vibration amplitude, and had little effect on critical speeds. The larger stiffness mainly increased the critical speeds, and had little effect on vibration amplitude, which was confirmed again in Fig. 11.

One perfect set of rotor dynamics parameters was selected for the spin test system. The k_1 586 N/m and c_1 1.7 N·s/m were the most appropriate in the four sets of dynamic parameters. Based on the tests above, the comparison between the calculated unbalance response and the experimental response indicated that the dynamic model was proper.

5. Rubbing and excitation experiment

The flywheel/stop rubbing experiments were done to verify the feasibility and the limitation of using stops to start up or control the large vibration of flywheels. The experimental rubbing conditions are basically designed to suit the numerical simulation parameters. The flywheel/stop gap is 0.2 mm. The vibration displacement x_3 of the flywheel top is mainly monitored, which is mainly because x_3 is larger than the lower damper vibration displacement x_1.

As the rubbing and excitation experiment had a strong dynamic nonlinearity, the modeling of an accurate nonlinear rubbing model was a follow-up work.

5.1. Rubbing to start-up

As shown in Fig. 12, the orbits showed the flywheel rotor contacted the stop occasionally at the beginning of rubbing to start-up. The vibration amplitude remained at almost the value of the gap when the stop acted, which was about 0.2 mm. The stop restricted the amplitude of the vibration very effectively with the rotating speed was increasing. the impact and the friction between the flywheel and the stop suppressed the vibration of the flywheel. When the motor speed reached about 960 rpm, the flywheel was rotating stably. The constant output of the rotation speed transducer indicated that the friction torque had not exceeded the motor-driven torque.

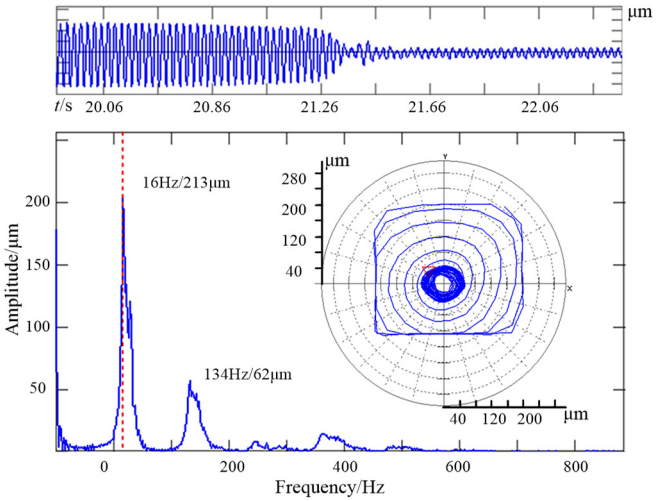

Fig. 12. Rubbing to start-up (gap = 0.2 mm)

The vibration waveform and orbits in Fig. 12 showed vibration energy of the flywheel was dissipated quickly through rubbing inside the gap between flywheel and stop. The stop would not act after rubbing to start up, which because the vibration amplitude was much smaller than the gap between the stop and flywheel. Fig. 12 showed the vibration amplitude was about 60 μm after rubbing to start up, while the gap was 0.2 mm.

The FFT analysis in Fig. 12 showed the shafting had two frequencies which were 16 Hz and 134 Hz. as shown in Fig. 3, the 1st-order and 2nd-order critical speeds are 900 rpm and 7800 rpm respectively. Obviously, the two frequencies were in good agreement with critical speeds by the simulation. The rotor rotated counterclockwise. Obviously, the vibration consisted of two kinds of rotation frequencies.

There are many dynamic parameters which may affect rubbing to start-up, such as stiffness of the stop, rubbing friction coefficient, gap, and so on. However, the gap's effect on rubbing to start-up will be discussed in this paper. The influences of other dynamic parameters on rubbing to start-up will be gradually studied in the follow-up.

Fig. 13 showed orbits of rubbing to start-up with four different gaps. It can be seen that the bigger gap had the longer time for rubbing to start-up. It took 9.6 s to rotate stably when the gap was 0.8 mm, while just 0.3 s when the gap was 0.2 mm. The shorter time will also reduce the damage to the stop and flywheel rotor. It is necessary to choose a smaller gap in the test.

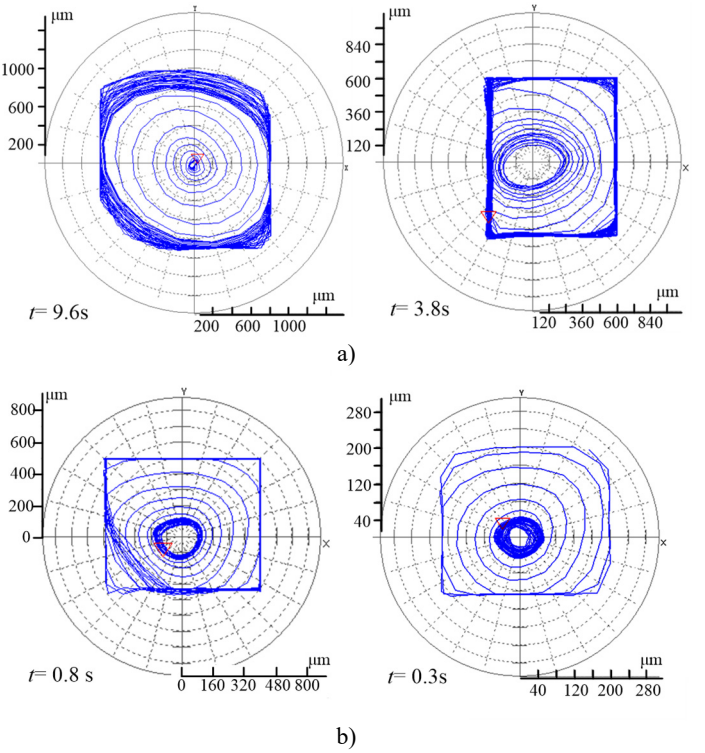

Fig. 13. a) gap = 0.8 mm and 0.6 mm, b) gap = 0.4 mm and 0.2 mm

5.2. Excitation to destruction

For the flywheel spin test, especially the composite flywheel endured high-speed centrifugal force, resin minor damages and fiber part breaks will produce non-ignorable disturbances, which causes shafting that has small modal damping ratios to natural whirl modes with low frequencies. Because the flywheel is rotating at a high speed in a spin test, the low frequency vibration will threaten flywheel life and structural strength seriously, such as causing rubbing to damage between stop and flywheel. It is necessary to study how and when the low-frequencies affect dynamic characteristics of the shafting.

The certain external harmonic excitation force was used to simulate the low frequency produced by sudden unbalances. The following steps were performed in the rubbing experiments. Firstly, the flywheel was brought to rubbing to start up and rotated steadily at the speed of 3000 rpm. The rubbing inside the gap was induced by low frequency excitation force, which was at the top of the flywheel in the x_1 direction. The magnitude and direction of the excitation force were adjustable and had the properties of harmonics. The use of low frequency excitation force was mainly based on the following reasons. It can be seen from Fig. 7 that the mode damping ratio of conical mode was very small, which had poor dynamic stability. Using low frequency excitation to induce conical mode was easy to achieve.

The exciter is an electromagnetic actor. It was set close to the flywheel top to perturb the magnetic field. The sinusoid signal from the signal generator was amplified and then drove the exciter to generate a synchronous harmonic excitation. the frequency of the excitation and the

amplitude vary to satisfy the experiments. to measure the excitation amplitude, a DC volt was applied to the electromagnetic actor, which led to the flywheel drifting off the central axis of the bearings. Then a compensation elastic force pushes the flywheel to its original center position. on measuring the elastic force, one obtains the relation between the DC volt and the force.

Firstly, the flywheel was brought to rubbing to start up and rotated steadily at the speed of 3000 rpm. The transducers and data test systems measured and recorded the dynamic behavior of the rotating flywheel, including the vibration time history, the frequency spectrum of vibration and the orbits of the flywheel center. Fig. 14(a) and (b) showed the shafting was in a motion of period 1. The axis orbit was a regular ellipse. The FFT analysis showed there was only one speed frequency.

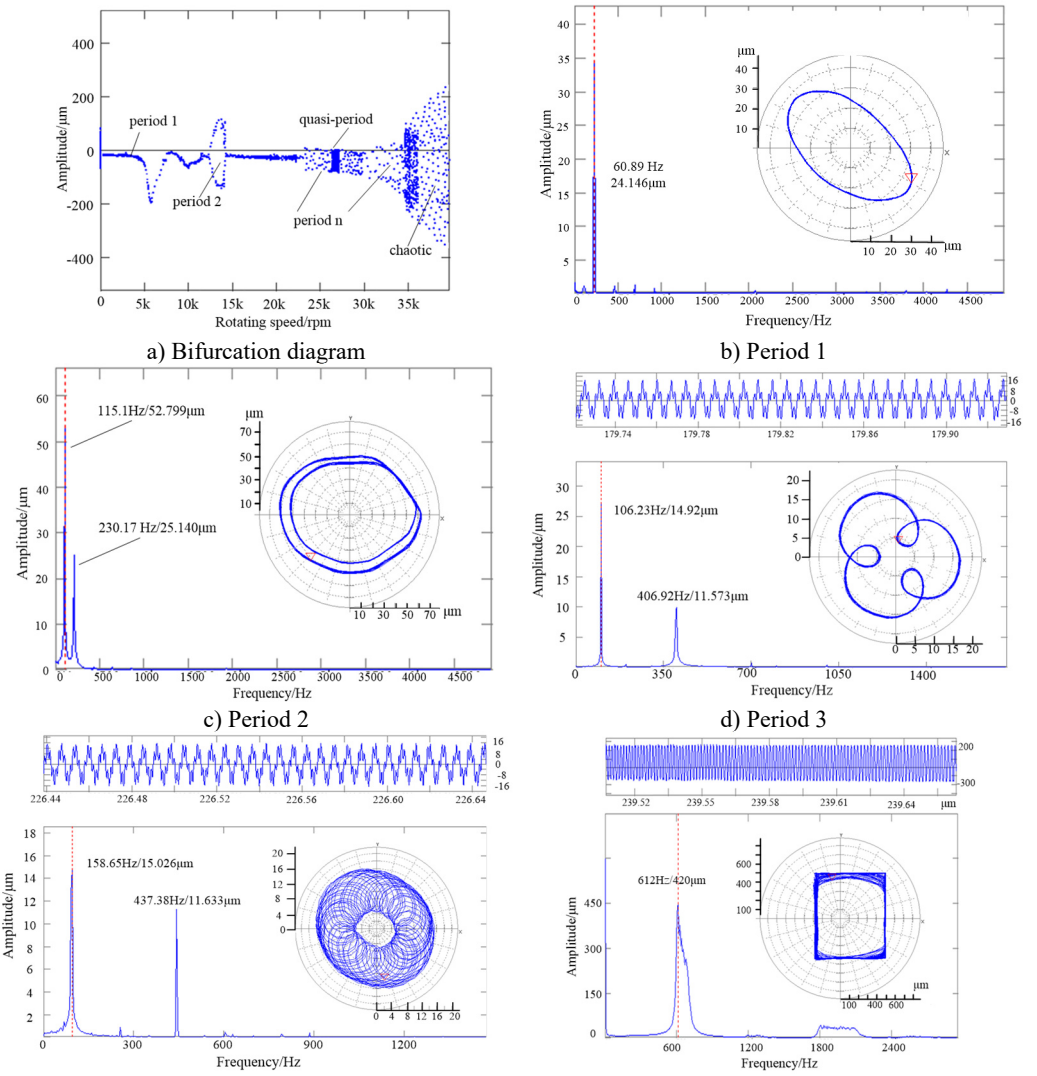

Fig. 14. The route of excitation to destruction

Then the proper excitation frequency of 115.1 Hz was found to obtain a large response of the flywheel top when the flywheel was rotating at a speed of 230.17 r/s. at that frequency, the excitation force was increased until the peak amplitude of flywheel whirl became larger and larger.

The flywheel/stop gap was adjusted to 0.3 mm, which was much larger than the vibration amplitude of the flywheel in normal operation. It can be seen from Fig. 14(a) and (c) the shafting went into period-doubling bifurcation motion. The periodic motion was composed of two low frequency motions, which were 115.1 Hz and 230.17 Hz individually. Obviously, the motion behavior was similar to the half frequency whirl, and the frequency of 115.1 Hz was being very near to the second order critical frequency 130 Hz. It can be seen from Fig. 14(a) the shafting reentered in a motion of period 1 when the excitation frequency and excitation force were canceled.

Fig. 14(d) was the vibration waveform of the flywheel excited by the excitation frequency of 106.23 Hz, and the orbit of the flywheel center was also shown in Fig. 14(d). The vibration amplitude was not large enough to exceed the gap between the flywheel and the stop. Spectrum analysis indicated that the vibration without rubbing was the double-frequency whirl composed of the excitation frequency 106.23 Hz whirl with large amplitude 14.92 μm and the synchronic 406.9 Hz whirl with small amplitude 11.57 μm. at that frequency, the shafting went into period 3 bifurcation motion. at the same way the shafting went into quasi-period motion when the proper excitation frequency was 158.65 Hz as shown in Fig. 14(e). It can be inferred that the excitation frequency was basically around the 2nd-order critical speed. It was indirectly proved that the mechanical model was proper.

The flywheel/stop gap was adjusted to 0.3 mm, which was much larger than the vibration amplitude of the flywheel in normal operation. The vibration amplitude was becoming larger as the excitation force increased. the excitation frequency was keeping around 130 Hz, which was near to the second order critical speed. When the speed reached to 36000 rpm, the motion was evolved from quasi-periodic motion to chaotic motion. The amplitude was getting bigger and bigger, and the axis orbit was becoming more and more chaotic till the full rubbing happened. The full rubbing was accompanied by a continuous collision and friction inside the gap. The center of the flywheel moved counter-clockwise and whipped in the amplitude exceeding the rotor/stop gap dramatically.

The vibrating flywheel went into whipping at a much higher frequency with amplitudes larger than the flywheel/stop gap. The flywheel rolled on the stop without separation. The continuous full rubbing slowed down the rotating speed of the flywheel. in order to observe the full rubbing behavior, the drive power of the motor was keeping large enough. The rubbing speed was increasing slowly. It can be seen from Fig. 14(a) and (f) the orbit of the flywheel center was like a square. The vibration signal consisted of two kinds of periodic motion by spectrum analysis. The rotating speed frequency was 612 Hz, and the high frequency band excited by rubbing was 1800-2200 Hz. The rotating speed frequency was 612 Hz, and corresponding vibration amplitude was 420 μm which was larger than the flywheel/stop gap. the excitation low frequency was not found when the rubbing occurred. It was inferred the exciter probe had been damaged. However, the broadband signal was observed, which located between 1800 Hz and 2200 Hz, and corresponding vibration amplitudes were about dozens of microns. The bifurcation diagram showed that the flywheel was in chaotic motion from Fig. 14(a).

When the drive power was cut off, the test rotating speed of the flywheel dropped from 36720 rpm down to nearly 0 rpm in 8.6 s because of the continuous flywheel/stop friction. After the rubbing experiments, a lot of metal powder was found on the inner face of the flywheel top, which meant that the continuous serious friction destroyed the contact surface of the flywheel and the stop. It was supposed that the full rubbing occurred at high speed would directly damage the stop and flywheel top. It was difficult to suppress sub-harmonic whirl of the flywheel when the rubbing occurred at high speed. The rubbing to start up suggested that the stop worked effectively only at a low speed for rubbing to start up.

6. Conclusions

1) The lower support of the flywheel shafting was composed of pivot jewel bearing and oil damper. the stiffness of pivot was very small. The oil damper provided viscous damping for the

flywheel shafting. The stop at the flywheel top was used to start up by rubbing. the dynamic model of the flywheel-bearing-damper system was built by means of the Lagrangian equation. The Campbell diagram, critical speeds, mode shapes, and modal damping ratios were calculated at different speeds. The numerical simulation indicated the exchange of mode shapes occurred in a narrow frequency range was a new kind of dynamic characteristics produced by flexible damping support. Through the analysis of the modal damping ratio, the dynamics of the flywheel shafting system was stable when the stop acted or not.

2) The comparison between the calculated unbalance response and the experimental response indicates that the dynamic model is appropriate. The experiments on the flywheel/stop rubbing demonstrated that the stop suppressed the low-frequency whirl successfully when rubbing to start up. the flywheel/stop rubbing was to make shafting rotating steadily. The bigger gap had the longer time for rubbing to start-up. The shorter rubbing time will also reduce the damage to the stop and flywheel rotor. It was necessary to choose a smaller gap in the test. The certain external harmonic excitation force was used to simulate the low frequency produced by sudden unbalances. In the very wide speed range, the low external harmonic excitation made the flywheel shafting produce period 1, period 2 bifurcation, period N and quasi-period motions. When the low-frequency excitation was cancelled, the flywheel shafting could resume stable operation and had not low and high frequencies except rotating frequency.

3) When the exciting force exceeds a certain value at high rotating speed, the quasi-periodic motion will change to chaos motion, and then the full rubbing occurs with continuous collision and friction inside the gap. the center of flywheel rotor moves counter-clockwise, and the whirl amplitude exceeds the gap unexpectedly. Moreover, the rubbing frequency is much higher than that of the excitation and the unbalance force. the rotor rotation is broken quickly by the stop. The full rubbing should be prevented since it damages the flywheel and stop directly.

Acknowledgement

This work was supported by the National Natural Science Foundation of China (Grant No. 11402267).

References

[1] **Bitterly J. G.** Flywheel technology: past, present, and 21st century projects. IEEE Aerospace and Electronic Systems Magazine, Vol. 13, Issue 8, 1998, p. 13-16.

[2] **Amine J., Cossi R. A., Bruno S., et al.** Sizing and energy management of a hybrid locomotive based on flywheel and accumulators. IEEE Transactions on Vehicular Technology, Vol. 58, Issue 8, 2009, p. 3947-3958.

[3] **Bo Y., Yuri M., John D., et al. on the** use of energy storage technologies for regulation services in electric power systems with significant penetration of wind energy. Electricity Market, 2008, p. 1-6.

[4] **Hamsic N., Schmelte A., Mohd A.** Increasing renewable energy penetration in isolated grids using a flywheel energy storage system. Powering, 2007, p. 195-200.

[5] **Yang K., Yang N., Xing C. W., et al.** Space-time network coding with transmit antenna selection and maximal-ratio combining. IEEE Transactions on Wireless Communications, Vol. 14, Issue 4, 2015, p. 2106-2117.

[6] **Ge C., Sun Z. L., Wang N., et al.** Energy management in cross-domain content delivery networks: a theoretical perspective. IEEE Transactions on Network and Service Management, Vol. 11, Issue 3, 2014, p. 264-277.

[7] **Han F. X., Zhao S. J., Zhang L., et al.** Survey of strategies for switching off base stations in heterogeneous networks for greener 5G systems. IEEE Access, Vol. 4, 2016, p. 4959-4973.

[8] **Serrano P., Costa Perez X., Wu J. S., et al.** Special issue: green communications. Computer Networks, Vol.78, 2015, p. 1-3.

[9] **Hu H. G., Wu J. S.** New constructions of codebooks nearly meeting the welch bound with equality. IEEE Transactions on Information Theory, Vol. 60, Issue 2, 2014, p. 1348-1355.

[10] **Arvin A. C., Bakis C. E.** Optimal design of press-fitted filament wound composite flywheel rotors. Composite Structures, Vol. 72, Issue 1, 2006, p. 47-57.
[11] **Li Y. L., Dai X. J., Zhang X. Z.** Research on process stress for circumferential wound composite flywheel rotors. Journal of Mechanical Strength, Vol. 32, Issue 2, 2010, p. 265-269.
[12] **Krack M., Secanell M., Mertiny P.** Cost optimization of hybrid composite flywheel rotors for energy storage. Structural and Multidisciplinary Optimization, Vol. 41, Issue 5, 2010, p. 779-795.
[13] **Tzeng J., Emerson R., Moy P.** Composite flywheels for energy storage. Composites Science and Technology, Vol. 66, 2006, p. 2520-2527.
[14] **Dai X. J., Tang C. L., Yu S. Q.** Measuring friction coefficient of the high speed pivot bearing in oil-bath lubrication by a varying load method. Tribology, Vol. 31, Issue 1, 2011, p. 7-11.
[15] **Tang C. L., Dai X. J. the** analysis on anti-wear properties advantage of high speed improved pivot-jewel bearing. Machine Design and Research, Vol. 26, Issue 5, 2010, p. 67-70.
[16] **Dai X. J., Zhang K., Tang C. L.** Friction and wear of pivot jewel bearing in oil-bath lubrication for high rotational speed application. Wear, Vol. 302, Issues 1-2, 2013, p. 1506-1513.
[17] **Ehrich F.** High order sub harmonic response of high speed rotors in bearing clearance. ASME Journal of Vibration, Acoustics, Stress and Reliability in Design, Vol. 110, 1988, p. 9-16.
[18] **Yanabe S., et al.** Rotor vibration due to collision with annular guard during passage through critical speed. Journal of Vibration and Acoustics, Vol. 120, Issue 2, 1998, p. 544-550.
[19] **Choy F. K., Padovan J.** Rub interaction of flexible casing rotor systems. ASME Journal of Engineering for Gas Turbine and Power, Vol. 111, Issue 4, 1989, p. 652-658.
[20] **Goldman P., Muszynska A.** Dynamic effects in Mechanical structures with gaps and impacting: order and chaos. ASME Journal of Vibration and Acoustics, Vol. 116, Issue 4, 1994, p. 541-547.
[21] **Jiang J., Ulbrich H.** Stability analysis of sliding whirl in a nonlinear Jeffcott rotor with cross-coupling stiffness coefficients. Nonlinear Dynamics, Vol. 24, Issue 3, 2001, p. 269-283.
[22] **Qin W. Y., Chen G. R., et al.** Nonlinear response of a rub-impact overhung rotor. Chaos, Solitons and Fractals, Vol. 19, Issue 5, 2004, p. 1161-1172.
[23] **Chu F. L., Lu W. X.** Experimental observation of nonlinear vibrations in a rub-impact rotor system. Journal of Sound and Vibration, Vol. 24, Issue 10, 2003, p. 970-973.
[24] **Yuan Z. W., Chu F. L., Hao R. J.** Simulation of rotor's axial rub-impact in full degrees of freedom. Mechanism and Machine Theory, Vol. 42, Issue 7, 2007, p. 763-775.
[25] **Zhang G. F., Xu W. N., Xu B., et al.** Analytical study of nonlinear synchronous full annular rub motion of flexible rotor-stator system and its dynamic stability. Nonlinear Dynamics, Vol. 57, Issue 4, 2009, p. 579-592.

Changliang Tang received Ph.D. degree in Department of Engineering Physics from Tsinghua University, Beijing, China. Now he works as an Associate Researcher at the Institute of Engineering Thermophysics, Chinese Academy of Sciences. His current research interests are rotor dynamics and bearing technology, structural strength and mechanics of composite materials.

Dongjiang Han received Ph.D. degree in Institute of Engineering Thermophysics from Chinese Academy of Sciences. Now he works at Institute of Engineering Thermophysics. His current research interests include rotordynamics, dynamic stability.

Jinfu Yang received Ph.D. degree in North China Electric Power University. Now he works at Institute of Engineering Thermophysics. His current research interests include rotordynamics, dynamic stability.